Journal of Materials Chemistry A

Accepted Manuscript

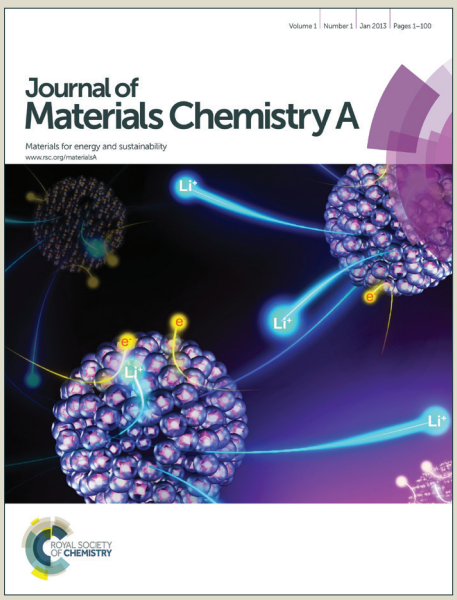

ROYAL SOCIETY OF CHEMISTRY

www.rsc.org/materialsA

Journal of Materials Chemistry A RSCPublishing

ARTICLE

Carbon–Supported Mo_2C Electrocatalysts for Hydrogen Evolution Reaction

Cite this: DOI: 10.1039/xoxxoooooox

B. Šljukić,[a] M. Vujković,[b] L. Amaral,[a] D.M.F. Santos,[a] R.P. Rocha,[c] C.A.C. Sequeira[a] and J.L. Figueiredo[c]

Received ooth January 2012,
Accepted ooth January 2012

DOI: 10.1039/xoxxoooooox

www.rsc.org/

Molybdenum carbide (Mo_2C) nanoparticles supported on two different carbon materials, carbon nanotubes and carbon xerogel, were prepared and characterised using X–ray diffraction, thermogravimetric analysis, scanning and transmission electron microscopy, nitrogen sorption and X–ray photoelectron spectroscopy. The analyses showed similar composition (*ca.* 27 wt.% of Mo_2C) and crystallite size (22–28 nm) of the two samples, but significantly different morphologies and specific surface areas. These were subsequently tested as electrocatalysts for hydrogen evolution reaction (HER) in acid media. Using linear scan voltammetry and electrochemical impedance measurements main reaction parameters were determined, including Tafel slope, charge transfer coefficient and exchange current density. Capacitance properties were examined and correlated with the electrocatalysts activity for HER. Stability of the two materials was also investigated and proved to be very good.

Introduction

Hydrogen (H_2) is seen as the most promising replacement of fossil fuels due to its high–energy content and no greenhouse gases evolution during its use.[1–4] Current main methods for H_2 production are based on fossil fuels,[2] while to take a full benefit of its advantages as clean fuel, it should be produced from a renewable energy source in a sustainable manner. Water electrolysis represents a simple and clean method for H_2 production,[5] but this process is too expensive at the moment. Its high cost results from high overpotential needed to operate the electrolysis cell and consequently, high energy consumption during the process. Overpotential value is related to electrode materials properties. Accordingly, cost of electrolytic H_2 production can be reduced by selecting inexpensive electrode materials on which hydrogen evolution reaction (HER) occurs at low overpotentials, *i.e.*, the HER is kinetically active.[6–9] In addition to the high electrocatalytic activity and low cost, electrodes to be used in water electrolysers should have large active surface area, electrochemical stability, good electrical conductivity and selectivity.[10] Furthermore, the electrode of choice should also have high corrosion resistance. During shut–down periods, the electrode materials can be corroded and consequently may lose their activity as well as life time. In view of that, it is very important to determine the corrosion behaviour of the electrode materials for application in industrial electrolysers.

HER on a metallic electrode S in acid media proceeds via two possible pathways, following either the Volmer–Heyrovsky or the Volmer–Tafel mechanism:[7]

$$S + H^+ + e^- \leftrightarrow S–H_{ads} \quad \text{(Volmer step)} \quad (1)$$

$$S–H_{ads} + H^+ + e^- \leftrightarrow H_2 + S \quad \text{(Heyrovsky step)} \quad (2)$$

$$S–H_{ads} + S–H_{ads} \leftrightarrow H_2 + 2S \quad \text{(Tafel step)} \quad (3)$$

Both mechanisms assume formation and then cleavage of the bond between metal and adsorbed hydrogen atom, $S–H_{ads}$. Therefore, the HER rate is determined by the strength of the bond of adsorbed proton to the metal surface with the maximum HER rate being achieved for intermediate $S–H_{ads}$ bond strength values (behaviour characterised by the well–known 'volcano plot').[11] Noble metals such as platinum (Pt) exhibit high catalytic activity for HER in acid media, but their high price and low abundance severely limit their large–scale application.[12,13] Transition metal carbides (TMC) are known to have Pt–like electronic and catalytic properties, but significantly lower cost.[14–16] Additionally, grafting of TMCs onto a high–surface area conductive support increases the ratio between their real and geometric surface area and thus improves their activity and efficiency for HER. Molybdenum (Mo) is considerably more abundant than noble metals[17] and its carbide is one of the most investigated TMCs due to its catalytic activity, good conductivity, high melting point and low cost.[18] Moreover, the onset potential for single–phase

[a] *Center of Physics and Engineering of Advanced Materials (CeFEMA), Instituto Superior Técnico, Universidade de Lisboa, 1049–001 Lisboa, Portugal.*
[b] *Faculty of Physical Chemistry, University of Belgrade, Studentski trg 12–16, 11158 Belgrade, Serbia.*
[c] *Laboratory of Catalysis and Materials – Associate Laboratory LSRE-LCM, Faculdade de Engenharia, Universidade do Porto, 4200–465 Porto, Portugal.*
Electronic Supplementary Information (ESI) available. See DOI: 10.1039/b000000x/
† Corresponding author: biljana.paunkovic@tecnico.ulisboa.pt

molybdenum carbide (Mo_2C) thin films oxidation in acid media is more positive than the HER onset potential.[19]
The aim of this study was to prepare Mo_2C supported on two different carbon supports – carbon nanotubes (CNTs) and carbon xerogel (CXG) – and to characterise their composition, structure and morphology. Subsequently, the materials' electrochemical activity for HER in acid media, as well as their long–term stability and corrosion behaviour, was investigated having in mind their possible applications as electrode materials for water electrolysers.

Experimental

Synthesis of carbon–supported Mo_2C

Molybdenum carbide (Mo_2C) nanoparticles were grafted on both carbon nanotubes (CNTs) and on carbon xerogel (CXG). First, aqueous solution of ammonium molybdate (0.788 g in 6 ml) was added dropwise to the carbon support (1 g), following a modified incipient wetness impregnation method, and the mixture was homogenised in an ultrasonic bath for 30 min. The samples were next dried at 110 ºC overnight. Carburisation was achieved in a tube furnace increasing the temperature from ambient to 800 ºC at 13 ºC min^{-1} under nitrogen flow, and then holding it at 800 ºC for 2 h. CNTs were purchased from NANOCYL™ (NC3100 series) and pre–treated with hydrochloric acid[20] prior to impregnation, while CXG was prepared by an adapted literature procedure.[21]

Characterisation of carbon–supported Mo_2C

Electrocatalysts structures were examined by XRD analysis with Philips 1050 Bruker D8 Advance with $CuK\alpha_{1,2}$ radiations in 10–80° 2θ range. Content of Mo_2C in the electrocatalysts was determined by performing thermogravimetric analysis (TGA)/differential thermal analysis (DTA) with TA SDT 2960 at a heating rate of 10 ºC min^{-1} under air flow. The morphology was examined by scanning electron microscopy (SEM) using JEOL JSM 7001F microscope and by transmission electron microscopy (TEM) using FEI Tecnai F30 instrument. Their textural characterisation was based on the nitrogen sorption analysis performed in a Quantachrome NOVA 4200e multi–station apparatus at −196°C. Surface areas of the carbon samples were determined according to the Brunauer–Emmett–Teller (BET) method and the average mesopore diameter (d_p) of the CXG sample was obtained by the Barrett–Joyner–Halenda (BJH) method. The mesopore surface area and micropore volume were calculated using t–method.

Electrochemical measurements

The working electrodes were prepared by uniformly depositing the corresponding catalytic ink on conductive substrates and drying them under vacuum at 120 ºC overnight. The catalytic inks were prepared by mixing Mo_2C/CNT or Mo_2C/CXG electrocatalyst powder (95%) with polyvinylidene fluoride (PVDF) binder (5%) in N–methyl 2–pyrrolidone (NMP) solvent. The electrocatalyst loading on the electrode was 8.2 and 6.3 mg cm^{-2} for Mo_2C/CNT and Mo_2C/CXG, respectively. Geometric area of the substrate was used to calculate the current densities.
Electrochemical measurements were done in a single–compartment glass cell with a Pt counter electrode and saturated calomel electrode (SCE) as reference. All the potentials in the paper are given relative to RHE. The electrocatalysts were tested for HER by recording linear scan voltammograms (LSV) in 0.1 M $HClO_4$ aqueous solutions at a scan rate of 0.5 mV s^{-1} and at temperatures ranging from 25 to 85 ºC. Electrochemical impedance (EI) measurements were carried out in 0.1 M $HClO_4$ in the frequency range of 100 kHz − 0.1 Hz at different HER overpotentials. Long–term stability tests were done by recording chronoamperograms (CAs) at constant potential at –0.2 V for 8 hours.

Results and Discussion

Characterisation of the carbon–supported Mo_2C

The formation of α–Mo_2C onto CNTs and onto CXG was confirmed by XRD analysis that was used to determine the crystal structure and average crystallite size. The XRD patterns (Fig. 1A) of both Mo_2C/CNT and Mo_2C/CXG showed a broad peak (2θ of *ca.* 26°) corresponding to carbon. The other peaks could be assigned to orthorhombic α–Mo_2C (ICSD card#1326) in both cases.

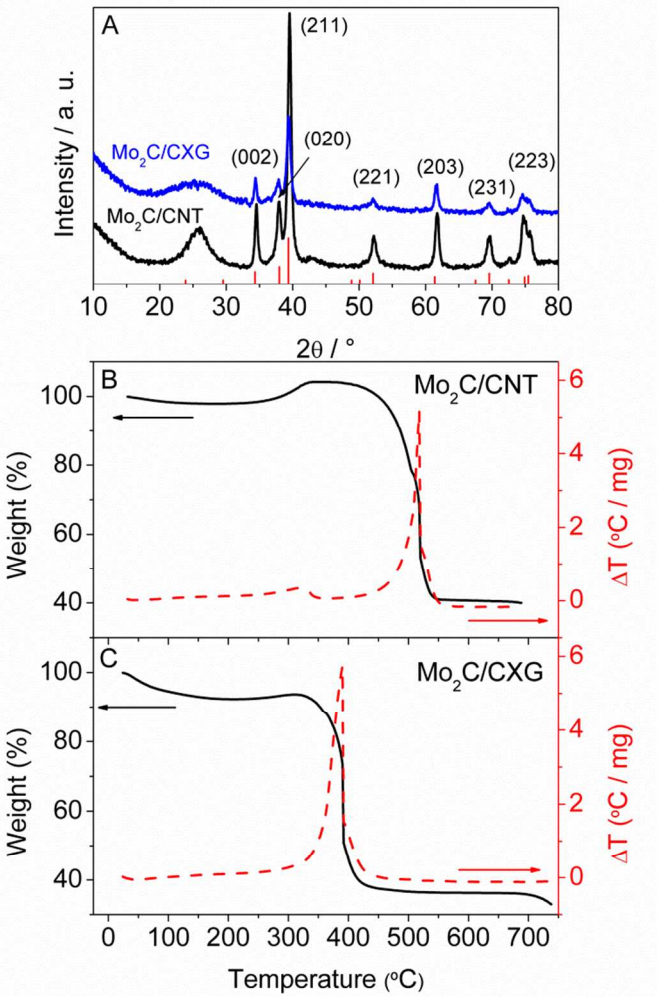

Figure 1. XRD patterns (A) and TGA curves of Mo_2C/CNT (B) and Mo_2C/CXG (C) electrocatalysts. ICSD card #1326 is also shown (A).

From the (211) peak data, crystallite sizes of 22.3 and 28.6 nm for Mo_2C/CNT and Mo_2C/CXG, respectively, were evaluated using Scherrer equation:[22]

$$d = \frac{0.9k_1}{B_{(2)}cos\theta} \quad (4)$$

where d stands for the average crystallite diameter, k_1 for the wavelength of the X–ray radiation (0.1541 nm), θ for the angle corresponding to the (211) peak, and $B_{(2)}$ for the width in radians of the diffraction peak at its half height.

TGA analysis (Fig. 1B and C) revealed that the amount of carbide formed was similar in both cases, *i.e.*, 28.5 and 25.6 wt.% of Mo_2C in case of Mo_2C/CNT and Mo_2C/CXG electrocatalyst, respectively. Comparison of TGA/DTA curves clearly shows that carbon combustion starts earlier with Mo_2C/CXG then with Mo_2C/CNT. This is a result of the more ordered structure of CNT compared to the carbon xerogel.

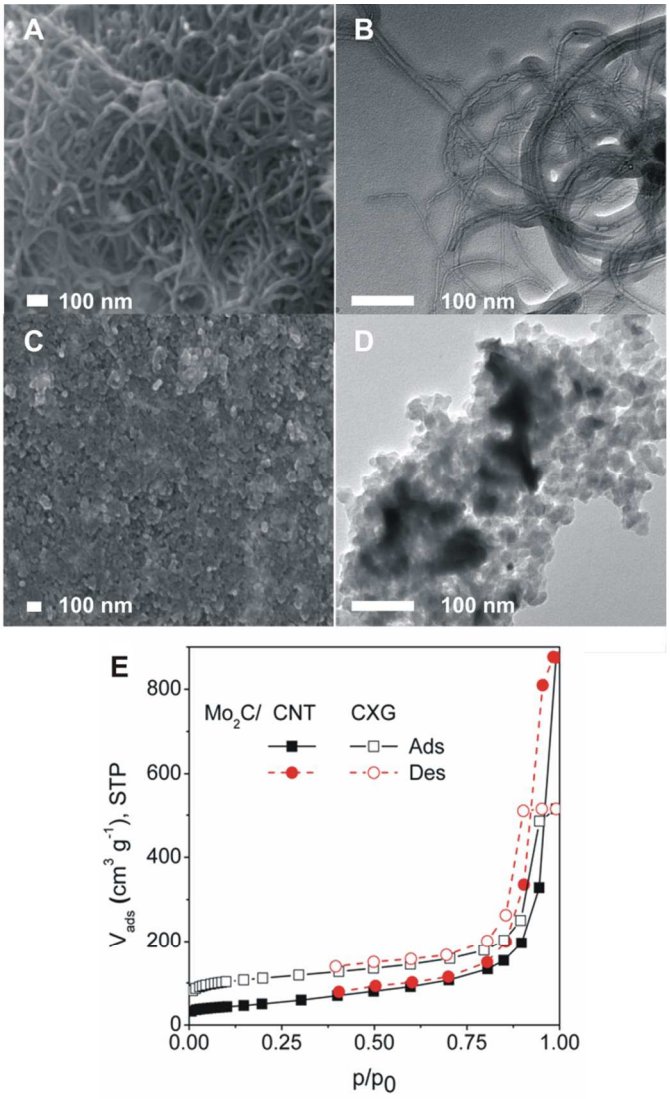

Figure 2. SEM and TEM images of Mo_2C/CNT (A and B, respectively) and Mo_2C/CXG (C and D, respectively) with their N_2–sorption isotherms at –196 °C (E).

The surface morphology of the catalysts was investigated by SEM and TEM. Secondary electron images shown in Fig. 2 reveal a quite different morphology, dependent on the carbon support. Mo_2C/CNT shows the characteristic tube-like morphology with the tube diameters ranging from 10 to 60 nm. The Mo_2C nanoparticles are observed to be dispersed on CNTs, while particles were found to be agglomerated to some extent rather than well dispersed in the case of Mo_2C/CXG.

Furthermore, N_2–sorption analysis revealed differences in the porosity and specific surface area values of the two electrocatalysts. Mo_2C/CNT was found to be non–porous with specific surface area of 182 m^2 g^{-1}. Conversely, Mo_2C/CXG was found to be predominantly mesoporous with average pore diameter around 18 nm and with some micropores present as well. Accordingly, large specific surface area of 410 m^2 g^{-1} was evaluated for Mo_2C/CXG.

The surface chemistry of the carbon–supported Mo_2C electrocatalysts was analysed by XPS, which revealed the presence of Mo in several oxidation states including the Mo 3d doublet located a 228.7 and 231.9 eV that is characteristic of Mo_2C.[23]

Carbon–supported Mo_2C activity for HER

Polarisation curves presenting current density, j, as a function of potential, E, were recorded for the two studied electrocatalysts in 0.1 M $HClO_4$ in the temperature range between 25 and 85 ºC (Fig. ESI–1). A reductive process could be observed when scanning the potential below 0.1 V, accompanied with the visible formation of H_2 bubbles. The polarisation curves showed typical Tafel behaviour, indicative of purely kinetically controlled HER.

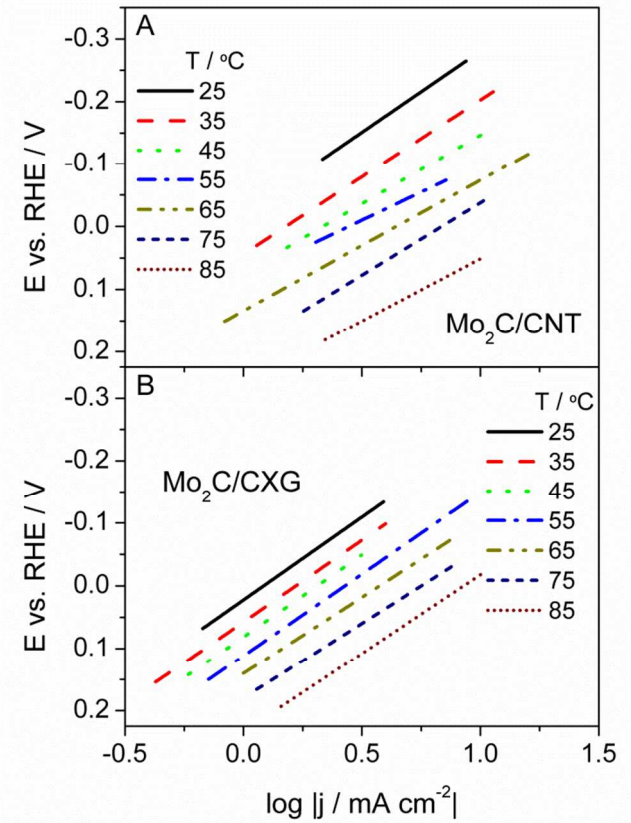

Figure 3. Tafel slopes of Mo_2C/CNT (A) and Mo_2C/CXG (B) in 0.1 M $HClO_4$ in the 25–85 ºC temperature range.

Subsequently, the data from the polarisation curves were used for construction of Tafel plots presenting dependence of overpotential, η, on log j, according to eqn (5) (Fig. 3).

$$\eta = a + b\log j = \frac{2.3RT}{\alpha F}\log j_0 - \frac{2.3RT}{\alpha F}\log j \quad (5)$$

where b is the Tafel slope, R is the universal gas constant, T is temperature, α is charge transfer coefficient, F is the Faraday constant and j_0 is the exchange current density.

j_0 values were calculated using the form of the Butler–Volmer equation for low overpotentials, considering the overpotential region between 0 and 0.01 V of the polarisation plots (eqn (6)).

$$\eta = \frac{RT}{j_0 F} j \quad (6)$$

At 25 ºC, similar b values of 251 and 264 mV dec^{-1} (no iR correction) were obtained for Mo_2C/CNT and Mo_2C/CXG, respectively. Suggested HER mechanisms in acidic media[7,24] assume Tafel slope value of *ca.* 120 mV dec^{-1} at 25 ºC if the Volmer reaction step, *i.e.*, adsorption of hydrogen (eqn (1)), is the rate determining step (RDS). Fast Heyrovsky step, *i.e.*, electrochemical desorption (eqn (2)), yields Tafel slope value of *ca.* 40 mV dec^{-1}, while fast Tafel step, *i.e.*, chemical desorption (eqn (3)) results in value of 30 mV dec^{-1}. Therefore, the polarisation curves indicate that the HER on carbon−supported Mo_2C electrocatalysts is controlled by the Volmer step, *i.e.*, by the rate of adsorption of hydrogen to form S−H_{ads}.

It could be noticed that the evaluated Tafel slope values are higher than expected for HER in acid media and generally higher than values reported when using other non–Pt electrocatalysts.[7] Some studies involving Mo_2C–based electrocatalysts report lower Tafel slope values for HER in acid media (up to 100 mV dec^{-1})[20,25–29] but higher values have been also previously reported (49–302 mV dec^{-1}),[30,31] Table 1. Comparison with different Mo compounds employed as electrocatalysts for HER in acid media (0.5 M H_2SO_4), revealed lower Tafel slope values in case of MoS_2 (98.8 mV dec^{-1}),[32] Ni_xS_y–MoS_2 (55.6 mV dec^{-1}),[32], MoS_x–graphene (43 mV dec^{-1}),[33] MoP (54 mV dec^{-1}),[34] MoP supported on carbon flakes (56.4 mV dec^{-1})[35] and Mo_2N (~100 mV dec^{-1}).[29] Accordingly, low α values of 0.23 and 0.22 were obtained for Mo_2C/CNT and Mo_2C/CXG, respectively. Tafel slope values higher than the theoretical ones indicate that electron flow through the material is possibly obstructed. Besides the crystal and electronic structures, the electrocatalysts morphology and particle size play determining roles in their catalytic activity for HER. Larger particle size (of μm order) and their irregular shape was reported to lead to higher Tafel slope values for HER at Mo_2C electrocatalyst.[36] Furthermore, presence of Mo oxides that can be formed during the carbides exposure to air and that are not efficient catalysts for HER, would lead to increased apparent Tafel slope values due to increased local resistance at the electrode−electrolyte interface.[36,37] Consequently, external energy input through the application of overpotential is used not only for HER itself, but also for overcoming electron transfer barrier. Accordingly, HER activation energy decrease is lower and, consequently, α values are lower.

Table 1. Performance of different Mo_2C–based electrocatalysts for HER in acid media

Electrocatalyst	Electrolyte	Method	b (mV dec^{-1})	j_0 (mAcm^{-2})	j_{200} (mAcm^{-2})	η_{10} (mV)
Mo_2C/CNT	0.1 M $HClO_4$	LSV	251	1.43	4.8	250
Mo_2C/CXG	0.1 M $HClO_4$	LSV	264	1.69	12.7	170
Mo_2C/CNT[20]	0.1 M $HClO_4$	EIS	55.2	1.4 x 10^{-2}	/	~152
Mo_2C/CXG[20]	0.1 M $HClO_4$	EIS	59.4	8.1 x 10^{-3}	~7.5	/
Bulk Mo_2C[20]	H_2–saturated 0.1 M $HClO_4$	EIS	87.6	6.0 x 10^{-4}	/	/
Mo_2C/NCNTs[25]	0.5 M H_2SO_4	EIS	71	1.98 x 10^{-2}	72.7	147
Mo_2C/CNTs[25]	0.5 M H_2SO_4	EIS	65	1.146 x 10^{-3}	24.1	179
Bulk Mo_2C[25]	0.5 M H_2SO_4	EIS	98	/	/	/
Mo_2C/CNT–GR[26]	0.5 M H_2SO_4	LSV	58	6.20 x 10^{-2}	/	130
Mo_2C/CNT[26]	0.5 M H_2SO_4	LSV	63	/	/	190
Mo_2C/GR[26]	0.5 M H_2SO_4	LSV	82	/	/	242
Mo_2C/C[26]	0.5 M H_2SO_4	LSV	66	/	/	212
Mo_2C/RGO[27]	0.5 M H_2SO_4	LSV	57.3	/	/	130
Mo_2C[27]	0.5 M H_2SO_4	LSV	76.7	/	/	/
Mo_2C NWs[28]	0.5 M H_2SO_4	LSV	55.8	/	10.2	/
Mo_2C NSs[28]	0.5 M H_2SO_4	LSV	64.5	/	5.3	/
Mo_2C[29]	0.5 M H_2SO_4	LSV, EIS	56	/	/	/
Mo_xC/Ni[30]	0.5 M H_2SO_4	LSV	49–302	0.01–0.35	/	/
Mo_2C[31]	0.05 M H_2SO_4	EIS	110–235	/		

η_{10} – overpotential driving current densities of 10 mA cm^{-2}; j_{200} – current density at overpotential of 200 mV; NCNTs − nitrogen doped CNTs; GR – graphene; RGO – reduced graphene oxide; NWs − nanowires; NSs − nanosheets

Similar j_0 values of 1.43 and 1.69 x 10^{-2} mA cm^{-2} were obtained for HER at Mo_2C/CNT and Mo_2C/CXG, respectively. These values are rather satisfactory for non−noble metal electrocatalysts. Furthermore, it should be noted that these values are of the same order of magnitude[20,26] or higher[31] than those reported for other carbon–supported Mo_2C electrocatalysts, and also 1−3 orders of magnitude higher than those normally reported for unsupported Mo_2C electrocatalysts.[36,38,39] Higher j_0 values are most likely due to the significantly larger specific surface area of carbon−supported Mo_2C electrocatalysts compared to the unsupported ones (BET surface area of 410 and 182 m^2 g^{-1} evaluated for the studied Mo_2C/CXG and Mo_2C/CNT, respectively, vs. 25 and 90 m^2 g^{-1} in the case of γ−Mo_2C and

β−Mo_2C, respectively)[39] resulting in higher number of active sites. Furthermore, increased electrical conductivity upon covalent binding of electrocatalysts with a carbon support was reported, as this covalent binding facilitates the electron transfer and reduces hydrogen bonding energy during HER.[20]

Electrochemical impedance analysis

Subsequently, impedance measurements were performed in order to further understand the two studied electrocatalysts activities for HER. The impedance plots of Mo_2C/CNT and Mo_2C/CXG measured at various negative potentials within the region corresponding to the LSV curves are shown in Fig. 4.

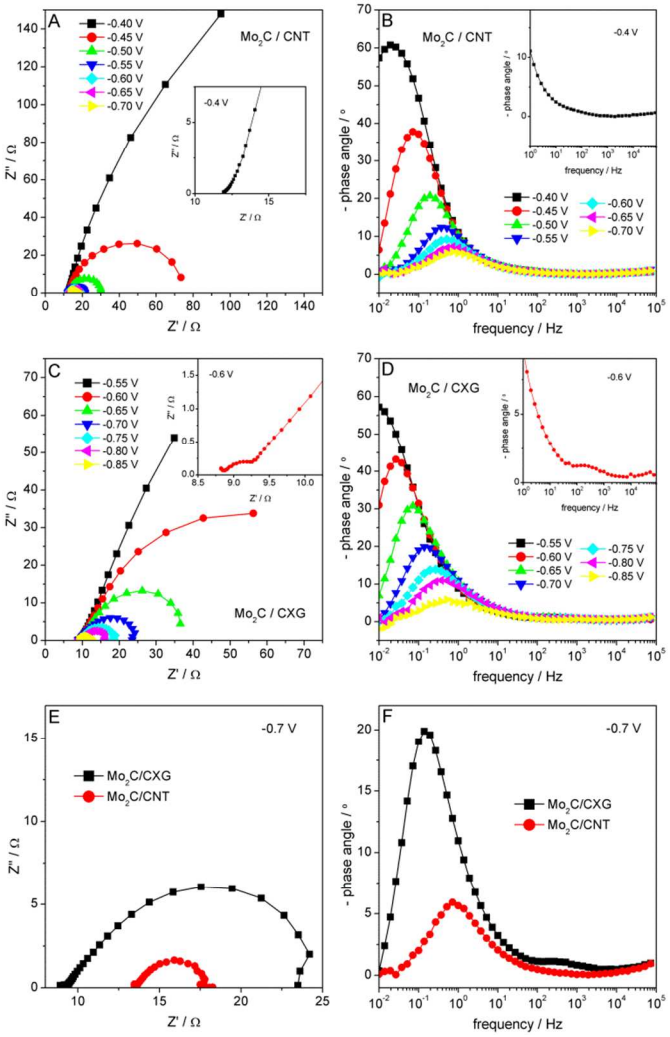

Figure 4. Nyquist and Bode plots of Mo_2C/CXG (A and B) and Mo_2C/CNT (C and D) measured at different potentials in 0.1 M $HClO_4$ with part of frequency region enlarged in the insets. Direct comparison of Nyquist (E) and Bode plots (F) of Mo_2C/CXG and Mo_2C/CNT measured at common applied potential is also included.

The Nyquist plots of Mo_2C/CXG reveal the occurrence of two−time constant processes as evidenced by two semicircles at all applied potentials. A small−diameter circle at high frequencies (inset in Fig. 4C), is related to the surface porosity, while the bigger one at lower frequencies corresponds to the charge–transfer resistance (R_{ct}) of the HER.[32] Namely, two time–constant model for description of HER assumes a resistance, R_s, in series with two parallel branches; first related to the charge-transfer process (C_{dl} – R_{ct}) and second related to the surface porosity. According to this model, R_s contains components arising from the resistance in the wiring (R_{wiring}), carbon support (R_{carbon}), resistance due to Mo_2C ($R_{carbide}$), and the solution resistance (R_{soln}).[32] Two processes, characterised with two relaxation times, are also evidenced in Bode plots of Mo_2C/CXG (Fig. 4D) as two waves at different frequencies. On the contrary, single–time constant process can be seen in impedance diagram of Mo_2C/CNT (Fig. 4). The absence of first semicircle in the Nyquist plots (inset in Fig. 4A) is a consequence of nonporous Mo_2C/CNT surface. Nyquist plot of both electrocatalysts showed that semicircle related to the charge transfer strongly depends of applied potential. Namely, R_{ct} decreased upon increase in overpotential. The corresponding changes were also observed in Bode plots.

The comparison of impedance response (Fig. 4E and F) at a common applied potential showed much faster charge transfer at Mo_2C/CNT than at Mo_2C/CXG electrocatalysts. The R_{ct} value, measured as the diameter of semicircles in Fig. 4E is significantly lower for Mo_2C/CNT CNT (~ 4 Ω) than that for Mo_2C/CXG CNT (~ 14 Ω), despite the lower specific surface area of Mo_2C/CNT. The porous surface favours higher double layer charging, thus promoting stronger hydrogen adsorption and the slower releasing of H_2 from active surface sites, as evidenced by the CV measurements (see below).

Double layer capacitance and hydrogen bonding

Additional CV measurements were carried out to obtain further details on charge storage capability of the two carbon–supported Mo_2C electrocatalysts in acid media and to better understand the complex processes at the electrode/electrolyte interface. The charging of double layer of Mo_2C/CNT and Mo_2C/CXG in 0.1 M $HClO_4$ within the potential region from 0.5 to 0 V, recorded using various scan rates, is presented in Fig. 5. Distortion of CV curve of Mo_2C/CXG could be observed at higher scan rates (50 and 100 mV s^{-1}), accompanied by decrease of double layer capacitance, originating from limited ability of electrolyte ions to penetrate into micropores at higher scan rates. Conversely, no change was observed in the shape of CVs of Mo_2C/CNT upon increasing of scan rates, as a consequence of the electrocatalysts non–porous surface. These different changes in the shape of the CV curves of the two electrocatalysts with the scan rate clearly indicate the role of carbon porosity in effective utilisation of surface area for double layer formation.[41,42]

Comparison of the CVs of Mo_2C/CXG and Mo_2C/CNT at scan rate of 20 mV s^{-1} demonstrated that Mo_2C/CXG possesses significantly higher double layer capacitance (Fig. 5C), due to the development of surface porosity. The ratio of capacitance values during cathodic scan between Mo_2C/CNT and Mo_2C/CXG at 20 mV s^{-1} is about 2.3, which corresponds exactly to the ratio of their specific surface areas. Enhanced electrocatalytic activity is favoured by increasing both surface area and capacitance since both lead to higher contact area of material with electrolyte. So, it is reasonable to expect that Mo_2C/CXG delivers faster HER compared to Mo_2C/CNT. However, the retardation of ions inside of pores cannot be neglected since it is known that narrow micropores represent strong bonding adsorption sites for hydrogen.[43]

When the cut–off potential from negative side was extended below the thermodynamic value of HER, *i.e.*, below ~0 V (Fig.

ESI–2), the reduction current of hydrogen evolution was observed, as well as the corresponding hump of oxidation of stored hydrogen. Shifting the potential cut–off up to –0.5 V by 100 mV steps (Fig. ESI–2A,B), the hump of hydrogen oxidation increased during each step of Mo_2C/CXG cycling, while this hump reached constant current value during the Mo_2C/CNT cycling. The penetration of hydrogen into Mo_2C/CXG pores probably contributes to the observed behaviour.

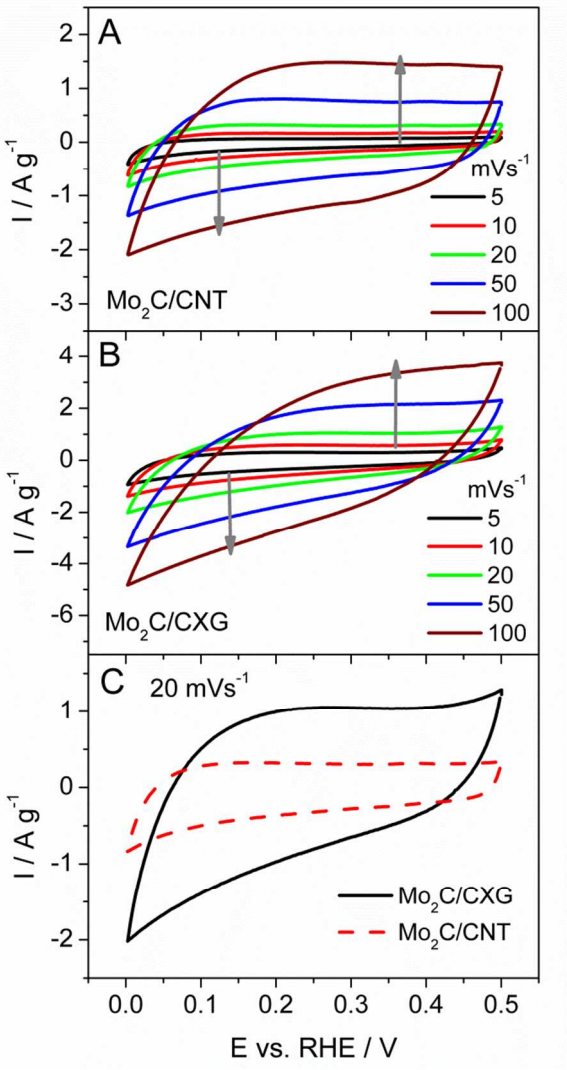

Figure 5. CVs of Mo_2C/CXG and Mo_2C/CNT measured at different scan rates. Comparison of their CV at 20 mV s^{-1} within same potential region.

The oxidation peak of stored hydrogen is positioned at negative potentials, for both materials, indicating that hydrogen is weakly chemisorbed at the catalyst surface. Hydrogen oxidation peak for Mo_2C/CNT corresponds approximately to the equilibrium theoretical value while in the case of Mo_2C/CXG it is shifted towards more positive value. That means that adsorbed hydrogen is more strongly bonded in Mo_2C/CXG than in Mo_2C/CNT and thus requires a higher overpotential for driving HER.

Stability tests

Finally, electrocatalysts durability and stability of their activity for HER in acid media was investigated. As mentioned, carbon materials represent good low−cost support due to their high surface area. However, their slow degradation in acid media has been pointed out as the main reason for electrocatalyst loss.[44] Therefore, long–term stability tests were performed by recording currents at constant potential for 8 hours. Both electrocatalysts exhibited good stability as evidenced by relatively constant current densities; actually, the current densities showed some increase after 2 hours, especially for Mo_2C/CXG. Additionally, polarisation curves of Mo_2C/CNT obtained before and after the stability tests (Fig. 6B) showed that kinetics was somewhat improved after the test and thus confirmed high stability of the electrocatalyst.

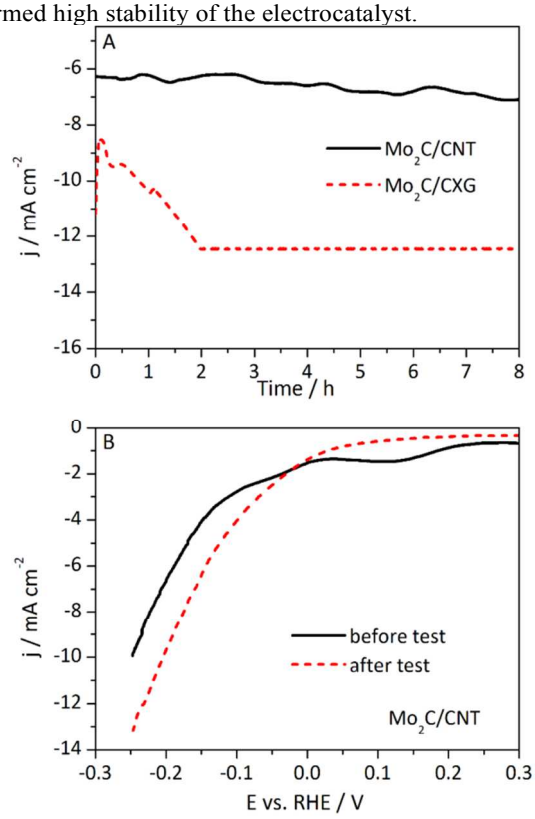

Figure 6. Chronoamperometric curves of Mo_2C/CNT and Mo_2C/CXG in 0.1 M $HClO_4$ at constant potential (A) and Mo_2C/CNT polarisation curves in 0.1 M $HClO_4$ before and after the stability tests (B).

Conclusions

α–Mo_2C was anchored on two different carbon supports, commercial CNTs and herein prepared CXG. The two materials were found to have similar crystallite size and composition (*ca.* 27 wt.% Mo_2C), but distinctively different morphology and specific surface area (410 m^2 g^{-1} for Mo_2C/CXG vs. 182 m^2 g^{-1} for Mo_2C/CNT). Evaluation of her activity for the two electrocatalysts in acid media indicates higher activity of Mo_2C/CNT compared to Mo_2C/CXG in the low overpotential region, and higher activity of Mo_2C/CXG for most of the tested potential domain. Study revealed higher HER current densities at Mo_2C/CXG compared to those at Mo_2C/CNT. Still, a

somewhat lower Tafel slope was evaluated for Mo_2C/CNT along with better charge transfer, possibly due to the more graphitic structure of the carbon nanotubes. Furthermore, stability tests showed very good performance of both electrocatalysts.

Acknowledgements

The authors thank the Foundation for Science and Technology (FCT, Portugal), for postdoctoral research grants SFRH/BPD/91853/2012 (D.M.F. Santos), SFRH/BPD/77768 /2011 (B. Šljukić), and SFRH/BPD/97453/2013 (L. Amaral), for PhD grant SFRH/BD/95411/2013 (R.P. Rocha), and for funding project "Functional materials for electrolytic hydrogen production" (PTDC/SEN–ENR/121265/2010), as well as to the Ministry of Education, Science and Technological Development of Republic of Serbia for support within the project No. III45014. LSRE-LCM was co-financed by FCT and FEDER under Program PT2020 (Project UID/EQU/50020/2013).

Notes and references

1. J. A. Turner, *Science*, 2004, **305**, 972−974.
2. D. M. F. Santos, B. Šljukić, C. A. C. Sequeira, D. Macciò, A. Saccone and J. L. Figueiredo, *Energy*, 2013, **50**, 486–492.
3. A. B. Laursen, S. Kegnaes, S. Dahl and I. Chorkendorff, *Energy Environ. Sci.*, 2012, **5**, 5577−5591.
4. M. T. M Koper and E. Bouwman, *Angew. Chem. Int. Ed.*, 2010, **49**, 3723−3725.
5. N. A. Kelly, *Hydrogen production by water electrolysis*, in A. Basile and A. Iulianelli, eds, Advances in *Hydrogen Production, Storage and Distribution*, Woodhead Publishing, 2014, p. 159–185.
6. T. G. Kelly, S. T. Hunt, D. V. Esposito and J. G. Chen, *Int. J. Hydrogen Eng.*, 2013, **38**, 5638–5644.
7. E. Navarro–Flores, Z. Chong and S. Omanovic, *J. Molecul. Catal. A: Chem.*, 2005, **226**, 179–197.
8. D. M. F. Santos, C. A. C. Sequeira, D. Maccio, A. Saccone, and J. L. Figueiredo, *Int. J. Hydrogen Eng.,* 2013, **38**, 3137–3145.
9. D. M. F. Santos, L. Amaral, B. Šljukić, D. Macciò, A. Saccone and C.A.C. Sequeira, *J. Electrochem. Soc.*, 2014, **161**, F386–F390.
10. B. Yazici, G. Tatli, H. Galip and M. Erbil, *Int. J. Hydrogen Eng.*, 1995, **20**, 957–965.
11. I. E. L. Stephens and I. Chorkendorff, *Angew. Chem. Int. Ed.*, 2011, **50**, 1476.
12. M. J. Liao, Z. D. Wei, S. G. Chen, L. Li, M. B. Ji and Y.Q. Wang, *Int. J. Hydrogen Eng.*, 2010, 35 (2010) 8071.
13. H. H. Hwu and J.G. Chen, *Chem. Rev.*, 2005, **105**, 185−212.
14. A. L. Tomás–García, J. O. Jensen, N. J. Bjerrum and Q. Li, *Electrochim. Acta*, 2014, **137**, 639–646.
15. S. Press in Encyclopedia of Global Resources, Vol. 3 (Ed.: C. W. Allin), Pasadena, 2010, pp. 772 – 775.
16. W-F. Chen, J. T. Muckerman, E. Fujita, *Chem. Comm.*, 2013, **49**, 8896−8909.
17. W. Zheng, T. P. Cotter, P. Kaghazchi, T. Jacob, B. Frank, K. Schlichte, W. Zhang, D. S. Su, F. Schueth and R. Schloegl, *J. Am. Chem. Soc.*, 2013, **135**, 3458–3464.
18. E. C. Weigert, D. V. Esposito and J. G. Chen, *J. Power Sources*, 2009, **193**, 501–506.
19. M. E. Eberhart and J. M. MacLaren, in: S. T. Oyama, ed. *The Chemistry of Transition, Metal Carbides and Nitrides*, Blackie, Glasgow, 1996, ch. 5, p. 107–120.
20. W. F. Chen, C. H. Wang, K. Sasaki, N. Marinkovic, W. Xu, J. T. Muckerman, Y. Zhu and R. R. Adzic, *Energy Environ. Sci.*, 2013, **6**, 943–951.
21. N. Job, R. Pirard, J. Marien and J.–P. Pirard, *Carbon*, 2004, **42**, 619–628.
22. B. E. Warren, *X–Ray diffraction*, Addison–Wesley, Reading, MA, 1969.
23. F. Solymosi, A. Oszkó, T. Bánsági and P. Tolmacsov, *J. Phys. Chem. B*, 2002, **106**, 9613–9618.
24. B. Borresen, G. Hagen and R. Tunold, *Electrochim. Acta*, 2002, **47**, 1819–1827.
25. K. Zhang, Y. Zhao, D. Fu and Y. Chen, *J. Mater. Chem. A*, 2015, **3**, 5783-5788.
26. D. H. Youn, S. Han, J. Y. Kim, J. Y. Kim, H. Park, S. Choi and J. S. Lee, *ACS Nano*, 2014, **8**, 5164–5173.
27. L. F. Pan, Y. H. Li, S. Yang, P. F. Liu, M. Q. Yua and H. G. Yang, *Chem. Comm.*, 2014, **50**, 13135–13137.
28. C. Gea, P. Jiang, W. Cui, Z. H. Pu, Z.i Xing, A. M. Asiri, A. Y. Obaid, X. Sun,, J. Tian, *Electrochim. Acta*, 2014, **134**, 182–186.
29. L. Ma, L. R. L. Ting, V. Molinari, C. Giordano, B. S. Yeo, *J. Mater. Chem. A*, 2015, **3**, 8361–8368.
30. J. Zhang, X. Meng, J. Zhao, Z. Zhu, *Chem. Cat. Chem*., 2014, **6**, 2059–2064.
31. N. S. Alhajri, D. H. Anjum and Kazuhiro Takanabe, *J. Mater. Chem. A*, 2014, **2**, 10548−10556.
32. Wei Cui, C. Ge, Z. Xing, A. M. Asiri, X. Sun, *Electrochim. Acta*, 2014, **137**, 504−510.
33. Z. Pu, Q. Liu, A. M. Asiri, A. Y. Obaid, X. Sun, *J. Power Sources*, 2014, **263**, 181−185.
34. Z. Xing, Q. Liu, A. M. Asiri, X. Sun, *Adv Mater*., 2014, **26**, 5702−5707.
35. W. Cui, Q. Liu, Z. Xing, A. M. Asiri, K. A. Alamry, X. Sun, *App. Catal. B: Enviromen.*, 2015, **164**, 144−150.
36. H. Vrubel and X. Hu, *Angew. Chem. Int. Ed.*, 2012, **51**, 12703−12706.
37. A. L. Tomás−García, J. O. Jensen, N. J. Bjerrum and Q. Li, *Electrochim. Acta*, 2014, **137**, 639−646.
38. W. Cui, N. Cheng, Q. Liu, C. Ge, A. M. Asiri and X. Sun, *ACS Catal.*, 2014, **4**, 2658−2661.
39. C. Wan, Y. N. Regmi and B. M. Leonard, *Angew. Chem. Int. Ed.*, 2014, **53**, 6407−6410.
40. B. Losiewicz, A. Budniok, E. Rowinski, E. Lagiewka and A. Lasia, *Int. J. Hydrogen Eng.*, 2004, **29**, 145–157.
41. J. Chmiola, G. Yushin, Y. Gogotsi, C. Portet, P. Simon and P. L. Taberna, *Science*, 2006, **313**, 1760–1763.
42. M. Vujković, N. Gavrilov, I. Pašti, J. Krstić, J. Travas–Sejdić, G. Ćirić–Marjanović and S. Mentus, *Carbon*, 2013, **64**, 472–486.
43. K. Jurewitz, E. Frackowiak and F. Beguin, *Appl. Phys. A*, 2004, **78**, 981–987.
44. D. V. Esposito, S. T. Hunk, Y. C. Kimmel and J. G. Chen, *J. Am. Chem. Soc.*, 2012, **134**, 3025−3033.